THE JOURNAL OF PHYSICAL CHEMISTRY C

Article

pubs.acs.org/JPCC

(2n × 1) Reconstructions of TiO_2(011) Revealed by Noncontact Atomic Force Microscopy and Scanning Tunneling Microscopy

Chi Lun Pang,*[,†] Ayhan Yurtsever,*[,‡,§] Jo Onoda,[‡] Yoshiaki Sugimoto,[‡] and Geoff Thornton[†]

[†]Department of Chemistry and London Centre for Nanotechnology, University College London, London WC1H 0AJ, United Kingdom

[‡]Graduate School of Engineering, Osaka University, 2-1 Yamada-Oka, Suita, Osaka 565-0871, Japan

[§]Institute of Scientific and Industrial Research, Osaka University, 8-1 Mihogaoka, Ibaraki, Osaka 567-0047, Japan

ABSTRACT: We have used noncontact atomic force microscopy (NC-AFM) and scanning tunneling microscopy (STM) to study the rutile TiO_2(011) surface. A series of (2n × 1) reconstructions were observed, including two types of (4 × 1) reconstruction. High-resolution NC-AFM and STM images indicate that the (4 × 1)-α phase has the same structural elements as the more widely reported (2 × 1) reconstruction. An array of analogous higher-order (2n × 1) reconstructions were also observed where n = 3−5. On the other hand, the (4 × 1)-β reconstruction seems to be a unique structure without higher-order analogues. A model is proposed for this structure that is also based on the (2 × 1) reconstruction but with additional microfacets of {111} character.

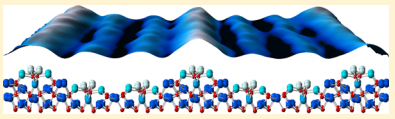

INTRODUCTION

TiO_2 has been investigated intensely since the 1970s when it was discovered that it is an active photocatalyst.[1] Although most surface science studies focus on the most thermodynamically stable rutile TiO_2(110) face,[2,3] there is a growing interest in other rutile terminations[4−18] as well as anatase TiO_2 surfaces.[19−21] The rutile TiO_2(011) surface has received particular interest because of a reportedly enhanced photoactivity.[22,23]

Most studies of TiO_2(011) report a (2 × 1) reconstruction, the structure of which was initially unclear, with two proposed models: a titanyl model[5] and a microfacet model.[6] However, three independent diffraction studies have clarified the surface structure,[9−11] all pointing to the "diffraction model" shown in Figure 1a. Theoretical calculations also find this to be the most stable of the proposed models.[9,10] Both the "beanlike" and "zigzag" motifs that appear in scanning tunneling microscopy (STM) images recorded "close to" and "far from" the surface, respectively,[10,15] could also be reproduced by STM images simulated from the "diffraction model".[15]

In addition to the (2 × 1) phase, Kubo et al.[6] also report noncontact atomic force microscopy (NC-AFM) and STM images of a coexisting (4 × 1) phase. Ahmed et al.[24] also report a (4 × 1) reconstruction following a wet preparation, but this phase does not survive a UHV anneal. Here, we report on a series of (2n × 1) reconstructions that are revealed by NC-AFM and STM images. Two types of (4 × 1) reconstruction were observed, which we refer to as (4 × 1)-α and (4 × 1)-β. The (4 × 1)-α surface has the same structural elements as the widely reported (2 × 1) reconstruction. In an analogous fashion, it is also possible to have an array of such (2n × 1) reconstructions; indeed, we observe a series of (2n × 1)-α reconstructions where n = 2−5. In contrast, the (4 × 1)-β reconstruction seems to be a unique structure without higher order analogues. The proposed structure for (4 × 1)-β has the same structural elements as the (2 × 1) phase but with the addition of {111} microfacets.

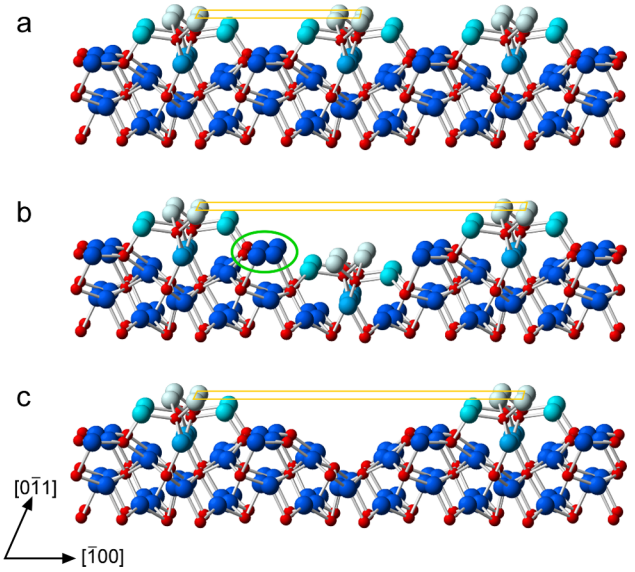

Figure 1. Ball and stick models of (a) the "diffraction model" for the TiO_2(011)-(2 × 1) phase,[9−11] (b) the model proposed for TiO_2(011)-(4 × 1)-α, and (c) the model proposed for TiO_2(011)-(4 × 1)-β. Red balls are Ti and blue balls are O. O atoms that form the (2n × 1) rows are shaded lighter. Surface unit cells are indicated in yellow and the green ellipse indicates the region between the added (2 × 1)-like rows where our NC-AFM and STM images do not show much detail.

Received: July 24, 2014
Revised: September 2, 2014
Published: September 8, 2014

   dx.doi.org/10.1021/jp507422s | J. Phys. Chem. C 2014, 118, 23168−23174

EXPERIMENTAL METHODS

The experiments were performed in Osaka using a custom-built NC-AFM housed in an ultrahigh-vacuum chamber (with a base pressure of ~5 × 10^{-11} Torr) and operated at room temperature. The TiO_2(011) crystal (Pi-Kem) was prepared using repeated cycles of Ar-ion bombardment (2 keV) for approximately 5 min and annealing between 1073 and 1273 K for 10−25 min. This gave the (2n × 1) terminations that we report. Preparation of a different TiO_2(011) crystal (MaTecK GmbH) with a lower annealing temperature of ~943−953 K led to the more commonly observed (2 × 1) termination. However, further systematic study is required to establish a definitive recipe for preparation of (2n × 1) terminations.

NC-AFM images were obtained using the frequency modulation detection method,[25] with the cantilever oscillation amplitude kept constant (peak-to-peak amplitudes 176−278 Å). The data presented here were taken with two silicon cantilevers which had resonant frequencies in the range ~155−156 kHz. A DC voltage (V_{CPD}) is added between the tip and sample that minimizes the average tip−sample contact potential difference.

STM images were obtained using the same cantilevers, biased with a voltage (V_s), with the oscillation still active such that the current is time-averaged ($\bar{I}_t$). In some cases, the tips were treated by electrical pulses or nanoindentation procedures to ensure sufficient conductivity for STM measurements.

RESULTS AND DISCUSSION

Structure of (2n × 1) Reconstructions. Figure 2a shows a large-area NC-AFM image of the TiO_2(011) surface. The image is characterized by a number of bright rows aligned to the [0$\bar{1}$1] direction. There are several domains present, which are shaded with different colors in Figure 2b. On the right-hand side, the rows have a (4 × 1) periodicity. The line profile in Figure 2c is obtained from the green line shown in Figure 2b, which crosses two (4 × 1) domains. It is clearly evident from the line profile that two types of (4 × 1) reconstruction are present: on the left-hand side, the corrugation of the rows is about 1.5 Å, whereas on the right-hand side, it is about twice this: ~3 Å. We refer to these as the (4 × 1)-α and (4 × 1)-β reconstructions, respectively. Apart from the greater corrugation of the (4 × 1)-β phase compared with (4 × 1)-α, the β phase can also be distinguished by its smoother appearance due to a lower density of defects, fixed (4 × 1) periodicity, and a broader appearance of the rows.

In Figure 2b, the (4 × 1)-α regions are unshaded, whereas the (4 × 1)-β region is shaded light-blue. The center of the image contains rows mostly with a (6 × 1) periodicity and a very narrow (2 × 1) domain that is shaded yellow. The (6 × 1) region is further separated into three domains, shaded light-red and dark-red. The unit cells of the two light-red regions contain two adjacent bright rows, whereas the unit cell of the dark-red region contains only one bright row. It is also apparent that the two light-red regions are out-of-phase with respect to each other, as highlighted by the white guideline in Figure 2b. This suggests that the bright rows in the regions shaded light- and dark-red are the same. In contrast to the (4 × 1)-β regions, it can also be seen that the other (2n × 1) regions merge with each other without discernible barriers. For instance, the row highlighted by the black guideline in Figure 2b going from top to bottom straddles (6 × 1), (2 × 1), and (4 × 1)-α regions.

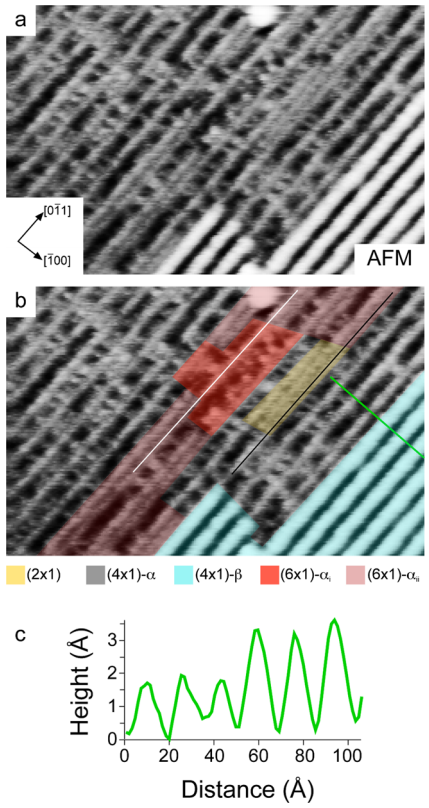

Figure 2. (a) NC-AFM image (350 Å × 226 Å, Δf = −1.5 Hz, V_{CPD} = 0.5 V) of the TiO_2(011)-(2n × 1) surface. (b) As (a) but annotated. Regions with different periodicities are shaded according to the key. The white and black lines are guidelines. (c) Line profile taken along the green line in (b) that shows a low corrugation for (4 × 1)-α and a greater corrugation for (4 × 1)-β.

On the basis that the rows from the (2n × 1) phases [apart from (4 × 1)-β] can simultaneously form part of the (2 × 1) and the higher order (2n × 1) phases, we propose that with the exception of (4 × 1)-β, all the bright rows from the (2n × 1) reconstructions have the same structure as that of the (2 × 1) reconstruction. As such, these phases will be referred to collectively as (2n × 1)-α. A series of schematic models for these (2n × 1)-α structures are shown in Figure 3a. By definition, if the added (2 × 1) rows are packed with saturation density, then the frequently reported (2 × 1) reconstruction will be formed.[5−16] When the spacing of the added rows is doubled, the (4 × 1)-α reconstruction is formed as shown in Figure 3a. Consistent with the NC-AFM image in Figure 2, where two types of (6 × 1)-α reconstruction were observed depending on how many bright rows are present (labeled (6 × 1)-α_i and (6 × 1)-α_{ii} in Figure 2b), two (6 × 1)-α models are shown in Figure 3a using either one or two added rows per unit cell.

The high-resolution NC-AFM image in Figure 4a reveals further substructure within the added rows. The rows have a zigzag motif reminiscent of that reported previously in STM images of the (2 × 1) surface.[5−16] The zigzag can be simply defined by a triangle as shown in Figure 4a and highlighted in Figure 4b. Measurements of the dimensions show that the triangle is isosceles in nature, the equal sides being ~3.8 ± 0.4 Å and the long side being 5.45 Å. The latter side is in line with the unit cell along the [0$\bar{1}$1] direction and used to calibrate the measurements. The dimensions of this triangle are remarkably

dx.doi.org/10.1021/jp507422s | J. Phys. Chem. C 2014, 118, 23168−23174

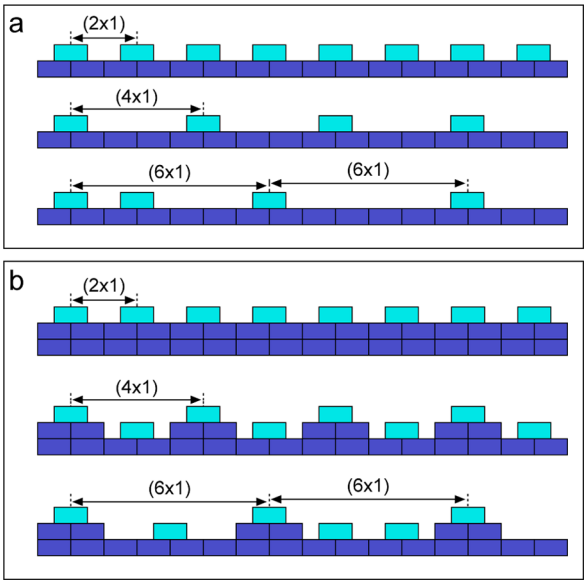

Figure 3. Schematic models of the $(2n \times 1)$-α phases. The models are constructed from (2×1) units shown light blue and unreconstructed (1×1) units in dark blue. In (a), the (2×1) units are on a flat (1×1) platform, whereas in (b), the second layer also contains (2×1) units.

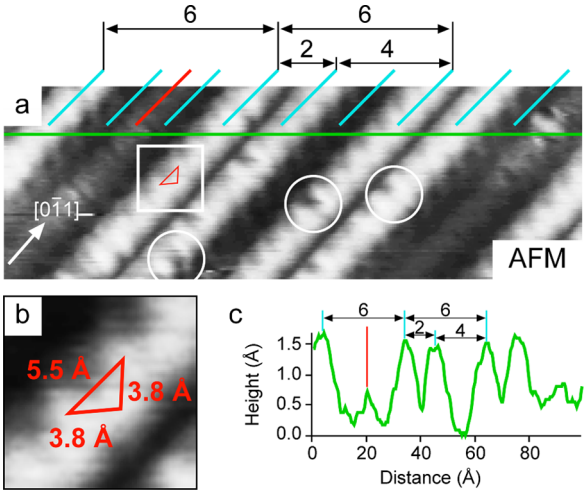

Figure 4. (a) NC-AFM image (100 Å × 35 Å, $\Delta f = -38.9$ Hz, V_{CPD} = 0.9 V) of TiO_2(011)-$(2n \times 1)$-α. The light blue lines indicate a 2× spacing with double-ended arrows indicating 2 × , 4 × , and 6× periodities. The red guideline marks one of the darker rows. A zigzag motif is observed that can be described by the isosceles triangle drawn red. A number of dark defects can be observed, some of which are circled in white. (b) Magnified part of the image shown in the white square in (a) with the measured dimensions. (c) Line profile taken from the green line in (a) that shows high peaks for the bright rows and lower peaks for the darker rows. One of the darker rows is marked with a red line. The same 2 × , 4 × , and 6× periodicities are marked as in (a).

close to those measured from STM images of the TiO_2(011)-(2 × 1) phase with zigzag contrast.[15]

Empty-state STM images taken from a similar area of the surface are shown in Figure 5. The same zigzag motif is discernible, and again, it can be described by an isosceles triangle with a long side of 5.45 Å and equal sides of ~3.9 ± 0.3 Å. This gives strong evidence to support our model where the

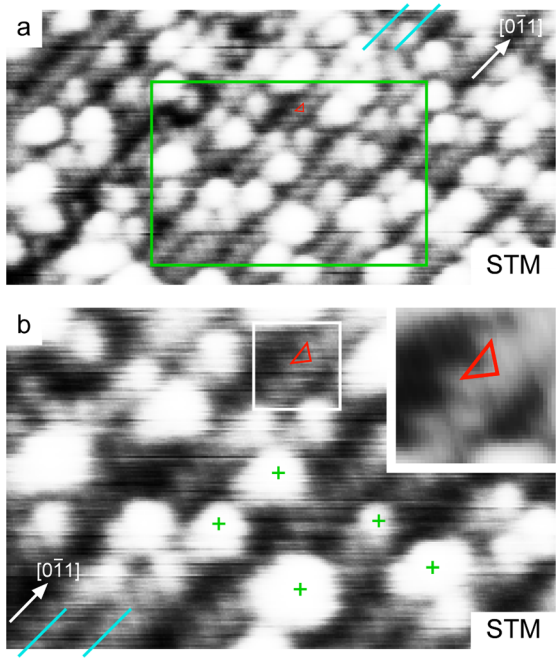

Figure 5. STM images of TiO_2(011)-$(2n \times 1)$-α with image parameters of (a) 200 Å × 100 Å, V_s = 3.5 V, $\bar{I}_t$ = 0.025 nA and (b) 100 Å × 62 Å, V_s = 3.5 V, $\bar{I}_t$ = 0.027 nA. The green rectangle in (a) marks the approximate area of the image in (b). Some point defects are marked with green crosses, and the light-blue lines mark some rows with (2 × 1) periodicity. The zigzag motif of the rows is highlighted by red triangles and the area marked by the white square is magnified in the inset. The image in the inset has an FFT filter applied to minimize the periodic noise and accentuate the zigzag motif.

added rows are composed of the same rows that form the (2 × 1) phase.

In empty-state STM, when the tip is relatively close to the sample, a beanlike contrast is found that is dominated by tunneling into O 2p states because the O atoms protrude further out of the surface. On the other hand, when the tip is further from the surface, the zigzag contrast is found. The zigzag contrast is dominated by tunneling into Ti 3d states because of its longer decay length compared to the O 2p states.[15] Given that the zigzag contrast is electronic in nature, it does not necessarily follow that a similar contrast should be seen in NC-AFM. However, a similar interplay between the decay of the tip−sample potential and the surface geometry could be at play, and theoretical calculations would shed more light on this. Note that at this stage, it is also not clear if the zigzag motif in NC-AFM arises from Ti, and this could be established by simultaneous measurement of NC-AFM and STM.

While evidence has been presented for the structure of the added rows of the $(2n \times 1)$-α reconstructions, the platform on which the added rows sit has not yet been discussed. The models in Figure 3a show these added rows on a (1 × 1) platform simply to highlight the periodicity of the added rows. However, inspection of Figure 4 shows that this is not necessarily the case. Two (6 × 1) units are marked in Figure 4a: one on the left-hand side and one in the center of the image. That on the left-hand side has a darker row (marked with a red line) as well as a bright row in the unit cell. The line profile in Figure 4c also shows this extra darker row clearly, the peak being about 1 Å lower than those of the bright rows.

dx.doi.org/10.1021/jp507422s | J. Phys. Chem. C 2014, 118, 23168−23174

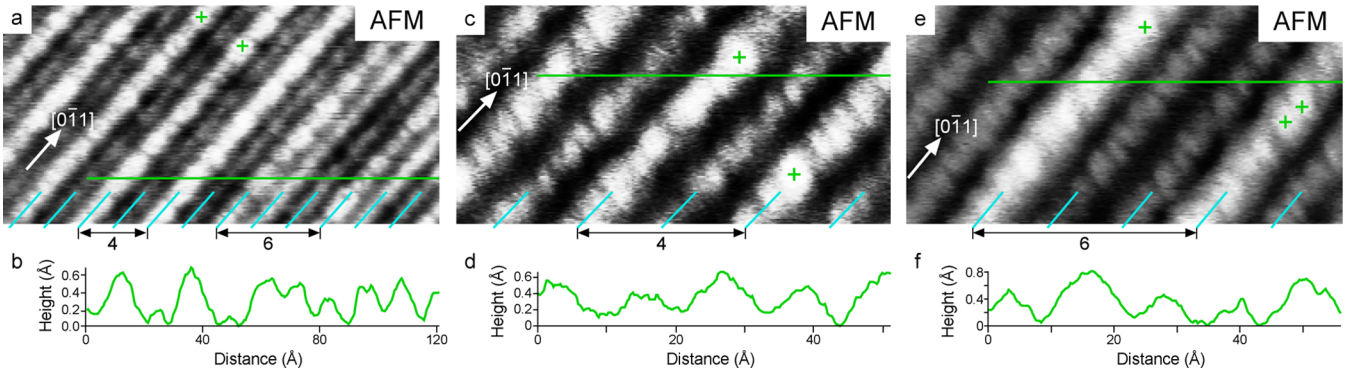

Figure 6. NC-AFM images and line profiles of TiO_2(011)-(2n × 1)-α. (a) Image parameters are 150 Å × 75 Å, Δf = −7.5 Hz, V_{CPD} = 0.6 V. (b) Line profile along the green line marked in (a). (c) Image parameters are 62.5 Å × 30 Å, Δf = −9.1 Hz, V_{CPD} = 0.6 V. (d) Line profile along the green line marked in (c). (e) Image parameters are 70 Å × 35 Å, Δf = −7.5 Hz, V_{CPD} = 0.6 V. (f) Line profile along the green line marked in (e). In (a), (c), and (e), the light-blue lines indicate a 2× spacing with double-ended arrows indicating 4× and 6× periodicities and green crosses marking the position of point defects. For easy comparison, the line profiles are drawn with the same x-axes scales as their corresponding images.

On the other hand, there does not appear to be an extra darker row between the added rows of the (4 × 1) part of the (6 × 1) structure in the center of the image. Figure 6a shows an NC-AFM image with a (4 × 1)-α region adjacent to a (6 × 1)-α region. The (4 × 1)-α region is clearly composed of alternating brighter and darker rows, also highlighted in the line profile in Figure 6b. Figure 6c shows a higher resolution image of the (4 × 1)-α region. The rows have an almost identical appearance, except the upper added rows are slightly broader. This is because they lie topographically higher and therefore part of their side structure is resolved. Likewise, in the NC-AFM image of the (6 × 1)-α region shown in Figure 6e, the unit cell consists of one bright row and two dark rows each with a similar appearance.

We therefore propose that the platform on which the added (2n × 1)-α rows stand can be either the unreconstructed (1 × 1) surface or rows with the (2 × 1) structure, as shown in the schematic models of Figure 3a,b, respectively. When n > 2, there are several configurations in which the (2 × 1)-like rows can be arranged to make the (2n × 1)-α structures. For instance, two types of (6 × 1) structure are shown in Figure 3b: (i) a structure that would appear in NC-AFM as one bright row and one darker row, as seen in Figure 4a, and (ii) a structure with one bright row and two darker rows, as observed in Figure 6e. A ball and stick model of the (4 × 1)-α structure (including a darker row) is shown in Figure 1b that corresponds to the schematic in Figure 3b. All other higher order (2n × 1)-α phases can be visualized using this model and arranging the units as shown in the schematics of Figure 3a,b. We note that while the scanning probe images give good evidence for the general structure proposed, the detailed structure between the rows is unknown (i.e., the region circled in green in the model of Figure 1b) and can probably be best addressed by computer modeling given that the structure does not have the long-range order required for quantitative diffraction studies.

Figure 7 shows a high-resolution image of the (4 × 1)-β phase. As with the images presented of the (2n × 1)-α phases, the row again has a zigzag motif. The zigzag can be described by an isosceles triangle similar to those in Figures 4b and 5b: the long side is ∼5.45 Å, and the shorter equal sides are ∼4.3 ± 0.3 Å, similar to that found for the (2n × 1)-α phases here and in STM images of the (2 × 1) termination.[15] The model we propose tentatively is therefore again based on elements of the "diffraction model" for the (2 × 1) phase. However, in this case, we remove every other row of the (2 × 1) model to create a microfaceted structure somewhat similar to that proposed by Kubo et al.[6] and illustrated in Figure 1c.

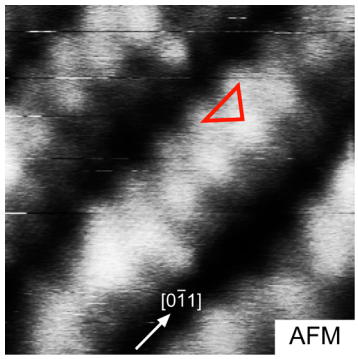

Figure 7. NC-AFM image (40 Å × 40 Å, Δf = −9.5 Hz, V_{CPD} = 0.6 V) of TiO_2(011)-(4 × 1)-β. The red triangle highlights the zigzag structure.

The proposed model would account for the greater corrugation observed in the NC-AFM images for this phase compared to the (2n × 1)-α phases. Such a microfaceted structure exposes the less stable {111} faces[18,26] and this could explain why the (4 × 1)-β structure does not develop further higher order structures like (6 × 1) and (10 × 1) because the proportion of the less stable {111} facets increases with the size of the microfacet. For the same reason, the (4 × 1)-β phase is likely to have a higher energy than the (2n × 1)-α phases. This could explain why when starting from an as-purchased crystal, the (4 × 1)-β phase was only observed during the first 21 sputter/anneal cycles, whereas the (2n × 1)-α phases were still observed after 64 cycles. In this scenario, the more stable (2n × 1)-α phases would tend to dominate upon repeated annealing. Note that while the (4 × 1)-β model can be created by removing (2 × 1) units from the (2 × 1) phase, this does not carry any implication on how the phase is formed. It may be that the reconstructions grow out from the surface as has been shown for the rutile TiO_2(110) surface.[27−30]

Defects on the (2n × 1)-α Reconstructions. In the high-resolution STM and NC-AFM images shown in Figures 4−6, several defects (or agglomerations of defects) can be seen, and some of these are marked with crosses and circles.

dx.doi.org/10.1021/jp507422s | J. Phys. Chem. C 2014, 118, 23168−23174

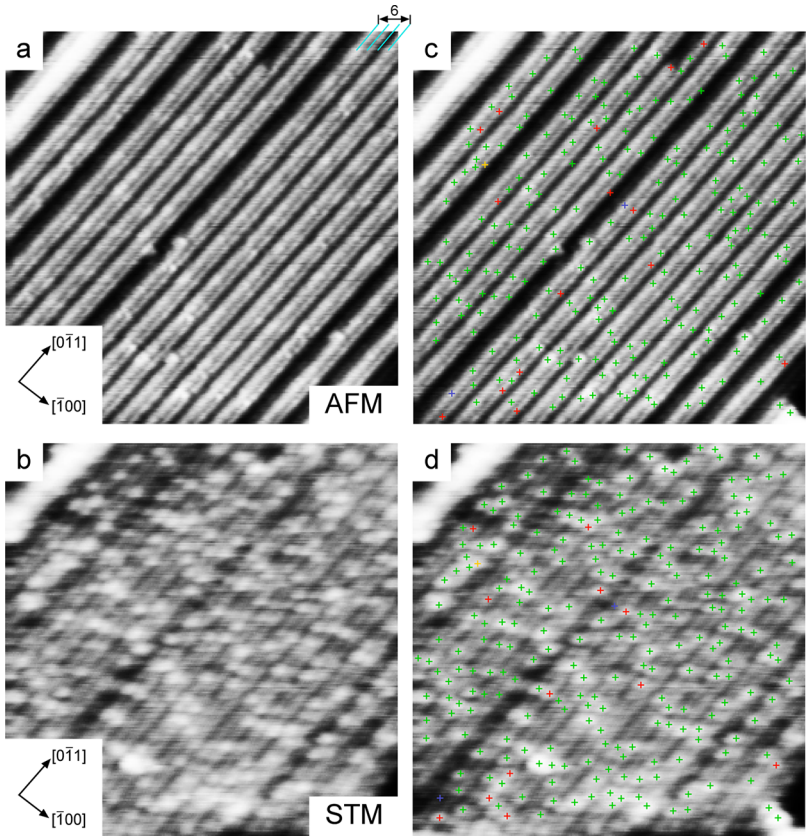

Figure 8. (a) NC-AFM image (350 Å × 350 Å, $\Delta f = -8.4$ Hz, $V_{CPD} = 0.9$ V) of $TiO_2(011)$-$(2n \times 1)$-α. The light-blue lines mark a 2× spacing, and the double-ended arrow marks the 6× periodicity; (b) STM image (350 Å × 350 Å, $V_s = 2$ V, $\bar{I}_t = 0.027$ nA) of the same area as (a); (c) and (d) are duplicates of (a) and (b), respectively. Green crosses mark defects present in both images, blue crosses mark defects visible in the NC-AFM image but not the STM image, red crosses mark defects visible in the STM image but not the NC-AFM image, and the yellow cross marks a defect that appears dark in the NC-AFM image but bright in the STM image.

Figure 8a,b show NC-AFM and STM images, respectively, that are taken from the same area of the surface in the vicinity of the images in Figures 4,5. This region has a predominantly (6×1) periodicity. Specifically, this region mainly has a (6×1)-α configuration where two bright rows make up the unit cell.

The green crosses in Figure 8 highlight coincident defects in the STM and NC-AFM image. In one case, a bright defect in the STM appears dark in the NC-AFM image and this defect is marked yellow. Red crosses indicate defects only seen in the STM image and blue crosses mark those that appear only in the NC-AFM image. The majority of crosses are green, indicating that most of the defects are detectable in both images. As the NC-AFM image was recorded 7 min after the STM image, at least some of the defects that cannot be matched between the images may arise from diffusion. Although dark defects that appear in STM images of $TiO_2(011)$-(2×1) with zigzag contrast have been assigned to oxygen vacancies,[7,8] bright defects have been assigned to adsorbed hydrogen.[14]

In sequential STM images and sequential NC-AFM images taken from the same area of the $TiO_2(011)$-$(2n \times 1)$-α phase (not shown), several of the bright defects change their positions, indicating that at least some of the defects can diffuse rather easily even at room temperature. On rutile $TiO_2(110)$ at room temperature, adsorbed hydrogen is known to diffuse either intrinsically or facilitated by molecular water.[31,32] On the other hand, diffusion of oxygen vacancies requires elevated temperature.[33] Given that the $(2n \times 1)$-α phase shares the same basic structure as $TiO_2(011)$-(2×1), the easy diffusion of the defects supports the assignment of the bright defects observed by Tao et al.[14] to adsorbed hydrogen.

As with images in STM,[34] it is well-known that the contrast obtained by NC-AFM can change depending on the nature of the tip apex.[35−39] The contrast changes can be drastic or more subtle. For instance, a subtle difference in contrast can be seen between the images in Figure 6a,c. Both NC-AFM images contain (4×1)-α regions with bright and darker rows. In the image in Figure 6a, the bright rows have a height of ∼0.6 Å, and the darker rows have a height of ∼0.2 Å, so that the height difference between them is ∼0.4 Å. On the other hand, in the image in Figure 6c, the bright rows have a height of ∼0.5 Å, and the darker rows have a height of ∼0.3 Å, with the height difference being only ∼0.2 Å. As such, the 4×1 periodicity in Figure 6a is clear, whereas the (4×1) periodicity in Figure 6c is only just discernible.

More drastic tip changes can be seen in the series of five NC-AFM images shown in Figure 9. These were recorded sequentially, and each image has a different contrast. In Figure 9a, the bright defects can be seen together with the bright $(2n \times 1)$-α rows. In Figure 9b, the contrast is similar, but the defects and rows appear more smeared out. The image appears similar to that in Figure 8a. In Figure 9c, there is a drastic contrast change: the $(2n \times 1)$-α rows still appear bright, but the contrast is only dark between rows with (2×1) periodicity. Between rows with a greater periodicity, there is a bright band. The defects are visible as very well-resolved bright spots, but the $(2n \times 1)$-α rows themselves are not resolved. In Figure 9d, the

dx.doi.org/10.1021/jp507422s | J. Phys. Chem. C 2014, 118, 23168−23174

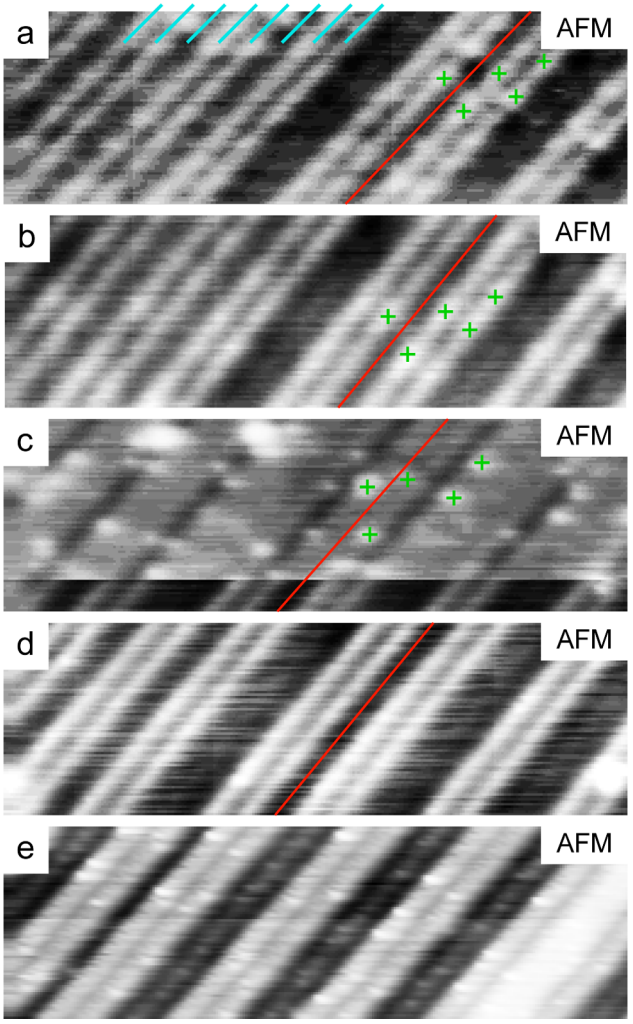

Figure 9. Sequential (200 Å × 60 Å, V_{CPD} = 0.9 V) NC-AFM images of TiO_2(011)-(2n × 1)-α with Δf = (a) −6.1 Hz, (b) −6.1 Hz, (c) −6.7 Hz, (d) −6.0 Hz, and (e) −5.8 Hz. The light-blue lines indicate a 2× spacing and in (a)−(d), the red guidelines mark equivalent rows. The red guidelines also mark the [0$\bar{1}$1] direction. The green crosses highlight some defects that are visible in (a)−(c). In (d), despite the image being more or less in the same area as (a)−(c), the defects are invisible, whereas the image in (e) was taken from a slightly different position.

contrast is similar to that in Figure 9b, but the (2n × 1)-α rows dominate, and the defects are invisible. Finally, in Figure 9e, there is another drastic tip change: the defects are again very well-resolved, but in contrast to the image in Figure 9c, the (2n × 1)-α rows are also well resolved.

The images in Figure 9 show that the point defects themselves can alter in appearance from very well-resolved to invisible. However, the contrast of these defects can also invert completely: although the defects presented in the images of Figures 6, 8 and 9 almost all appear bright, the defects in the image of Figure 4 appear as dark depressions.

It is clear that point defects on TiO_2(011)-(2n × 1)-α, and by extension TiO_2(011)-(2 × 1), can be resolved in NC-AFM. At least some of the defects are adsorbed hydrogen, but it is not yet clear if that is the only defect present. Furthermore, it is evident that like on the rutile TiO_2(110) surface,[35−39] several types of contrast are possible in NC-AFM. Both the origin of the different contrasts and the unambiguous assignment of defects could likely be resolved with further work combining STM and NC-AFM with theoretical simulation.[36,38]

CONCLUSIONS

In conclusion, we have used NC-AFM and STM to study the rutile TiO_2(011) surface. A series of (2n × 1) reconstructions were observed, including two types of (4 × 1) reconstruction: (4 × 1)-α and (4 × 1)-β. High-resolution NC-AFM and STM images suggest that the (4 × 1)-α phase has the same structural elements as the more widely reported (2 × 1) termination. Closely related higher-order (2n × 1)-α phases where n = 3−5 were also observed. The (4 × 1)-β reconstruction also has a structure based on the (2 × 1) reconstruction but with additional microfacets of {111} character. Higher-order analogues were not observed for the (4 × 1)-β phase. Although not definitively assigned, the same point defects were observed in both NC-AFM and STM images. In sequentially imaged areas, the NC-AFM contrast was subject to changes, and the point defects appeared clearer in some cases and invisible in others. Further study combining theoretical simulations with STM and NC-AFM may be able to explain such tip changes as well as identifying the point defects.

AUTHOR INFORMATION

Corresponding Authors

*E-mail: chi.pang@ucl.ac.uk. Fax: +44-207-679-0595. Tel: +44-207-679-5580.

*E-mail: ayhan@afm.eei.eng.osaka-u.ac.jp. Fax: +81-6-6879-7764. Tel: +81-6-6879-7763.

Notes

The authors declare no competing financial interest.

ACKNOWLEDGMENTS

The authors wish to thank Robert Lindsay for supplying the coordinates of the TiO_2(011)-(2 × 1) "diffraction model". This work was supported by a Grant-in-Aid for Scientific Research (20760024, 26110516, 26600015) from the Ministry of Education, Culture, Sports, Science and Technology of Japan (MEXT), Funding Program for Next Generation World-Leading Researchers, Osaka University Visiting Scholar Program, EU COST Action CM1104, the European Research Council Advanced Grant ENERGYSURF (to G.T.), the Royal Society (U.K.), and Alexander von Humboldt Stiftung (Germany).

REFERENCES

(1) Fujishima, A.; Honda, K. Electrochemical Photolysis of Water at a Semiconductor Electrode. *Nature (London)* **1972**, *238*, 37−38.

(2) Diebold, U. The Surface Science of Titanium Dioxide. *Surf. Sci. Reports* **2003**, *48*, 53−229.

(3) Pang, C. L.; Lindsay, R.; Thornton, G. Structure of Clean and Adsorbate-Covered Single-Crystal Rutile TiO_2 Surfaces. *Chem. Rev.* **2013**, *113*, 3887−3948.

(4) Pang, C. L.; Thornton, G. The Many Faces of Rutile Titania. *Surf. Sci.* **2006**, *600*, 4405−4406.

(5) Beck, T. J.; Klust, A.; Batzill, M.; Diebold, M.; Di Valentin, C.; Selloni, A. Surface Structure of TiO_2(011)-(2 × 1). *Phys. Rev. Lett.* **2004**, *93*, 036104.

(6) Kubo, T.; Orita, H.; Nozoye, H. Surface Structures of Rutile TiO_2(011). *J. Am. Chem. Soc.* **2007**, *129*, 10474−10478.

(7) Dulub, O.; Di Valentin, C.; Selloni, A.; Diebold, U. Structure, Defects, and Impurities at the Rutile TiO_2(011)-(2 × 1) surface: A Scanning Tunneling Microscopy Study. *Surf. Sci.* **2006**, *600*, 4407−4417.

(8) Dulub, O.; Batzill, M.; Solovev, S.; Loginova, E.; Alchagirov, A.; Madey, T. E.; Diebold, U. Electron-Induced Oxygen Desorption from the TiO_2(011)-2 × 1 Surface Leads to Self-Organized Vacancies. *Science* **2007**, *317*, 1052−1056.
(9) Torrelles, X.; Cabailh, G.; Lindsay, R.; Bikondoa, O.; Roy, J.; Zegenhagen, J.; Teobaldi, G.; Hofer, W. A.; Thornton, G. Geometric Structure of TiO_2(011)(2 × 1). *Phys. Rev. Lett.* **2008**, *101*, 185501.
(10) Gong, X.-Q.; Khorshidi, N.; Stierle, A.; Vonk, V.; Ellinger, C.; Dosch, H.; Cheng, H.; Selloni, A.; He, Y.; Dulub, O.; Diebold, U. The 2 × 1 Reconstruction of the Rutile TiO_2(011) Surface: A Combined Density Functional Theory, X-ray Diffraction, and Scanning Tunneling Microscopy Study. *Surf. Sci.* **2009**, *603*, 138−144.
(11) Chamberlin, S. E.; Hirschmugl, C. J.; Poon, H. C.; Saldin, D. K. Geometric Structure of TiO_2(011)(2 × 1) Surface by Low Energy Electron Diffraction (LEED). *Surf. Sci.* **2009**, *603*, 3367−3373.
(12) Tekiel, A.; Godlewski, S.; Budzioch, J.; Szymonski, M. Nanofabrication of PTCDA Molecular Chains on Rutile TiO_2(011)-(2 × 1) Surfaces. *Nanotechnology* **2008**, *19*, 495304.
(13) Tao, J.; Luttrell, T.; Batzill, M. A Two-Dimensional Phase of TiO_2 with a Reduced Bandgap. *Nat. Chem.* **2011**, *3*, 296−300.
(14) Tao, J.; Cuan, Q.; Gong, X.-Q.; Batzill, M. Diffusion and Reaction of Hydrogen on Rutile TiO_2(011)-2 × 1: The Role of Surface Structure. *J. Phys. Chem. C* **2012**, *116*, 20438−20446.
(15) Woolcot, T.; Teobaldi, G.; Pang, C. L.; Beglitis, N. S.; Fisher, A. J.; Hofer, W. A.; Thornton, G. Scanning Tunneling Microscopy Contrast Mechanisms for TiO_2. *Phys. Rev. Lett.* **2012**, *109*, 156105.
(16) Addou, R.; Senftle, T. P.; O'Connor, N.; Janik, M. J.; van Duin, A. C. T.; Batzill, M. Influence of Hydroxyls on Pd Atom Mobility and Clustering on Rutile TiO_2(011) −2 × 1. *ACS Nano* **2014**, *8*, 6321−6333.
(17) Ariga, H.; Taniike, T.; Morikawa, H.; Tero, R.; Kondoh, H.; Iwasawa, Y. Lattice-Work Structure of a TiO_2(001) Surface Studied by STM, Core-Level Spectroscopies and DFT Calculations. *Chem. Phys. Lett.* **2008**, *454*, 350−354.
(18) Uetsuka, H.; Henderson, M. A.; Sasahara, A.; Onishi, H. Formate Adsorption on the (111) Surface of Rutile TiO_2. *J. Phys. Chem. B* **2004**, *108*, 13706−13710.
(19) Setvín, M.; Aschauer, U.; Scheiber, P.; Li, Y.-F.; Hou, W.; Schmid, M.; Selloni, A.; Diebold, U. Reaction of O_2 with Subsurface Oxygen Vacancies on TiO_2 Anatase (101). *Science* **2013**, *341*, 988−991.
(20) De Angelis, F.; Di Valentin, C.; Fantacci, S.; Vittadini, A.; Selloni, A. Theoretical Studies on Anatase and Less Common TiO_2 Phases: Bulk, Surfaces, and Nanomaterials. *Chem. Rev.* **2014**, DOI: dx.doi.org/10.1021/cr500055q.
(21) Wang, Y.; Sun, H.; Tan, S.; Feng, H.; Cheng, Z.; Zhao, J.; Zhao, A.; Wang, B.; Luo, Y.; Yang, J.; Hou, J. G. Role of Point Defects on the Reactivity of Reconstructed Anatase Titanium Dioxide (001) Surface. *Nat. Commun.* **2013**, *4*, 2214.
(22) Rohrer, G. S. In *The Chemical Physics of Solid Surfaces: Oxide Surfaces*; Woodruff, D. P., Ed.; Elsevier: Amsterdam, 2001; Vol. *9*, Chapter 12.
(23) Ohno, T.; Sarukawa, K.; Matsumura, M. Crystal Faces of Rutile and Anatase TiO_2 Particles and their Roles in Photocatalytic Reactions. *New J. Chem.* **2002**, *26*, 1167−1170.
(24) Ahmed, M. H. M.; Lydiatt, F. P.; Chekulaev, D.; Wincott, P. L.; Vaughan, D. J.; Jang, J. H.; Baldelli, S.; Thomas, A. G.; Walters, W. S.; Lindsay, R. Wet Chemically Prepared Rutile TiO_2(110) and TiO_2(011): Substrate Preparation for Surface Studies under Non-UHV conditions. *Surf. Sci.* **2014**, *630*, 41−45.
(25) Albrecht, T. R.; Grütter, P.; Horne, D.; Rugar, D. Frequency Modulation Detection using High-Q Cantilevers for Enhanced Force Microscope Sensitivity. *J. Appl. Phys.* **1991**, *69*, 668−673.
(26) Ramamoorthy, M.; Vanderbilt, D.; King-Smith, R. D. First-Principles Calculations of the Energetics of Stoichiometric TiO_2 surfaces. *Phys. Rev. B* **1994**, *49*, 16721−16727.
(27) Onishi, H.; Iwasawa, Y. Dynamic Visualization of a Metal-Oxide-Surface/Gas-Phase Reaction: Time-Resolved Observation by Scanning Tunneling Microscopy at 800 K. *Phys. Rev. Lett.* **1996**, *76*, 791−794.
(28) Smith, R. D.; Bennett, R. A.; Bowker, M. Measurement of the Surface-Growth Kinetics of Reduced TiO_2(110) During Reoxidation using Time-Resolved Scanning Tunneling Microscopy. *Phys. Rev. B* **2002**, *66*, 035409.
(29) McCarty, K. F. Growth Regimes of the Oxygen-Deficient TiO_2(110) Surface Exposed to Oxygen. *Surf. Sci.* **2003**, *543*, 185−206.
(30) Pang, C. L.; Lindsay, R.; Thornton, G. Chemical Reactions on Rutile TiO_2(110). *Chem. Soc. Rev.* **2008**, *37*, 2328−2353.
(31) Li, S. C.; Zhang, Z.; Sheppard, D.; Kay, B. D.; White, J. M.; Du, Y.; Lyubinetsky, I.; Henkelman, G.; Dohnálek, Z. Intrinsic Diffusion of Hydrogen on Rutile TiO_2(110). *J. Am. Chem. Soc.* **2008**, *130*, 9080−9088.
(32) Wendt, S.; Matthiesen, J.; Schaub, R.; Vestergaard, E. K.; Laegsgaard, E.; Besenbacher, F.; Hammer, B. Formation and Splitting of Paired Hydroxyl Groups on Reduced TiO_2(110). *Phys. Rev. Lett.* **2006**, *96*, 066107.
(33) Zhang, Z.; Ge, Q.; Li, S.-C.; Kay, B. D.; White, J. M.; Dohnálek, Z. Imaging Intrinsic Diffusion of Bridge-Bonded Oxygen Vacancies on TiO_2(110). *Phys. Rev. Lett.* **2007**, *99*, 126105.
(34) Sánchez-Sánchez, C.; González, C.; Jelinek, P.; Méndez, J.; de Andres, P. L.; Martín-Gago, J. A.; López, M. F. Understanding Atomic-Resolved STM Images on TiO_2(110)-(1 × 1) Surface by DFT Calculations. *Nanotechnology* **2010**, *21*, 405702.
(35) Pang, C. L.; Sasahara, A.; Onishi, H.; Chen, Q.; Thornton, G. Noncontact Atomic Force Microscopy Imaging of Water Dissociation Products on TiO_2(110). *Phys. Rev. B* **2006**, *74*, 073411.
(36) Lauritsen, J. V.; Foster, A. S.; Olesen, G. H.; Christensen, M. C.; Kühnle, A.; Helveg, S.; Rostrup-Nielson, J. R.; Clausen, B. S.; Reichling, M.; Besenbacher, F. Chemical Identification of Point Defects and Adsorbates on a Metal Oxide Surface by Atomic Force Microscopy. *Nanotechnology* **2006**, *17*, 3436−3441.
(37) Yurtsever, A.; Sugimoto, Y.; Abe, M.; Morita, S. NC-AFM Imaging of the TiO_2(110)-(1 × 1) Surface at Low Temperature. *Nanotechnology* **2010**, *21*, 165702.
(38) Yurtsever, A.; Fernández-Torre, D.; González, C.; Jelínek, P.; Pou, P.; Sugimoto, Y.; Abe, M.; Pérez, R.; Morita, S. Understanding Image Contrast Formation in TiO_2 with Force Spectroscopy. *Phys. Rev. B* **2012**, *85*, 125416.
(39) Onoda, J.; Pang, C. L.; Yurtsever, A.; Sugimoto, Y. Subsurface Charge Repulsion of Adsorbed H-Adatoms on TiO_2(110). *J. Phys. Chem. C* **2014**, *118*, 13674−79.